

Bayesian Experimental Design for Model Discrepancy Calibration: A Rivalry between Kullback–Leibler Divergence and Wasserstein Distance

Huchen Yang, Xinghao Dong, Jin-Long Wu*

Department of Mechanical Engineering, University of Wisconsin–Madison, Madison, WI 53706

Abstract

Designing experiments that systematically gather data from complex physical systems is central to accelerating scientific discovery. While Bayesian experimental design (BED) provides a principled, information-based framework that integrates experimental planning with probabilistic inference, the selection of utility functions in BED is a long-standing and active topic, where different criteria emphasize different notions of information. Although Kullback–Leibler (KL) divergence has been one of the most common choices, recent studies have proposed Wasserstein distance as an alternative. In this work, we first employ a toy example to illustrate an issue of Wasserstein distance – the value of Wasserstein distance of a fixed-shape posterior depends on the relative position of its main mass within the support and can exhibit false rewards unrelated to information gain, especially with a non-informative prior (e.g., uniform distribution). We then further provide a systematic comparison between these two criteria through a classical source inversion problem in the BED literature, revealing that the KL divergence tends to lead to faster convergence in the absence of model discrepancy, while Wasserstein metrics provide more robust sequential BED results if model discrepancy is non-negligible. These findings clarify the trade-offs between KL divergence and Wasserstein metrics for the utility function and provide guidelines for selecting suitable criteria in practical BED applications.

Keywords: Bayesian experimental design, Wasserstein distance, Model discrepancy

1. Introduction

Quantifying the differences between probability distributions is a fundamental task across machine learning [1, 2], statistics [3, 4], biology [5, 6], and scientific computing [7, 8]. Various types of methods have been proposed for this purpose, including the family of f -divergences such as Kullback–Leibler (KL) and Jensen–Shannon (JS) divergences [9, 10, 11, 12], as well as integral probability metrics such as the Wasserstein, energy and Kolmogorov distances [13, 14, 15, 16].

In recent years, there has been a growing interest in exploring the Wasserstein distance as an alternative to the commonly used KL divergence in machine learning and statistical inference tasks [17, 18, 19]. In the field of generative models, it was shown in [20] that replacing KL- or JS-based losses with Wasserstein distance (e.g., in generative adversarial networks) leads to

*Corresponding author

Email address: jinlong.wu@wisc.edu (Jin-Long Wu)

more stable training and alleviates mode collapse, while [21] demonstrated that Wasserstein auto-encoders improve sample quality compared to standard VAEs that essentially rely on KL divergence. For variational inference, [22] proposed Wasserstein variational inference and showed that it remains stable even when the true and approximate distributions have disjoint supports, whereas [23] argued that sliced Wasserstein distance provides a proper metric and avoids the asymmetry and instability issues of KL divergence. In robust optimization, [24] analyzed KL-based distributional robustness and showed that it effectively reweights samples with higher losses to improve generalization guarantees, while [25] highlighted that Wasserstein distance naturally captures input perturbations and provides stronger robustness against adversarial attacks. In machine learning theory, [26] proved that Wasserstein-based generalization bounds are tighter than KL-based ones, and [27] further showed that Wasserstein distance provides guarantees for domain adaptation when the source and target distributions are close in this metric.

In Bayesian inference, the two distributions of interest are typically the prior and the posterior over latent quantities. The change from prior to posterior is interpreted as information gained from the data. Building on this perspective, Bayesian experimental design (BED) provides a principled framework for optimising data acquisition by leveraging Bayesian inference to guide the design process[28, 29, 30]. Rooted in information theory, BED aims to identify experimental conditions that maximize the expected information gain about target latent variables. This probabilistic approach not only ensures that experimental designs are tailored to the specific goals of the study but also allows for adaptive, sequential experimentation, where newly acquired data refine subsequent designs [31, 32, 33]. Various popular utility functions and criteria for selecting optimal designs have been summarized in [28, 34]. Among them, the KL divergence between the prior and posterior distributions [35, 36, 37] is one of the most common choices, as it provides a straightforward measure of the knowledge gain due to an experiment by quantifying the difference between two distributions. Formally, when the expectation is taken with respect to the prior predictive distribution of the data, this expected KL divergence coincides with the mutual information between the parameters and the observations [33, 38, 39].

Despite its popularity in Bayesian inference tasks to evaluate information gain, KL divergence also presents certain drawbacks. Its asymmetry, combined with the commonly adopted form “posterior relative to prior”, induces a statistical preference toward designs that concentrate posterior mass more sharply, rather than accounting for multiple plausible modes [40]. These characteristics are generally not problematic when the forward model is well specified. Because in these cases, the posterior mainly refines the prior by concentrating its mass within the main density region, without relocating it elsewhere. However, under model discrepancy [41, 42], where likelihood misspecification distorts the update, the posterior’s high-probability region may lie far from the prior’s [43, 44]. In such cases, the value of KL divergence can become extremely large, which in turn may cause the expected information gain to exhibit unstable gradients or to favor design choices that induce wrong posteriors [45]. Recent work has proposed using the Wasserstein distance, instead of the KL divergence, as the criterion for quantifying the difference between prior and posterior distributions [40] in BED. This work rigorously established that the expected Wasserstein utility is a well-posed and proper Bayesian information measure, satisfying key axioms such as sufficiency ordering. Among the various properties they highlight, two are particularly important in the context of experimental design: (i) the Wasserstein distance admits a clear geometric interpretation in terms of the optimal transport cost required to transform one distribution into another; and (ii) unlike KL divergence, it remains well-defined even when the prior and posterior

have non-overlapping supports, making it especially suitable for applications involving surrogate or empirical models.

The geometric interpretation of the Wasserstein distances (e.g., earth mover’s distance as 1-Wasserstein distance) leads to an important observation: starting from a uniform prior, moving all probability mass to two posterior distributions (e.g., Gaussian) of the same shape but centered at different locations incurs different transport costs. This behavior stands in sharp contrast to the KL divergence: for a uniform prior, two posteriors of the same shape yield the same value of KL divergence regardless of their relative location. This sensitivity of the Wasserstein distance to the absolute location of probability mass is not specific to BED. Several works in optimal transport and statistics have noted that classical Wasserstein distances are inherently sensitive to global translations [46, 47]. In some applications, such as comparing images or spatio-temporal fields, this sensitivity to global shifts has been viewed as a limitation, which has motivated the construction of translation-invariant or relative-translation-invariant variants of Wasserstein distance that explicitly factor out rigid displacements [48, 49]. These studies show that Wasserstein distances inherently couple shape and location information, in contrast to divergences that depend only on local density ratios. To the best of our knowledge, however, this location dependence of Wasserstein distances has not been systematically analyzed in the context of information gain via Bayesian inference, nor have its consequences for experimental design utilities been explored in detail.

On the other hand, the performance of BED relies on the accuracy of the forward model [32], while the model discrepancy [41, 50] is inevitable in most real-world applications. The model discrepancy primarily introduces errors in the forward evaluation of BED, leading to the following consequences: (i) introduction of bias in parameter estimation; (ii) continuous generation of similar designs and low-quality datasets, which present significant challenges in BED practice [43, 51, 44]. Although the recent developments of residual learning [52, 53, 54, 55, 45] are promising for characterizing the model discrepancy, they often involve neural networks with a large number of unknown coefficients. Although systematically gathering informative training data for network calibration could also be addressed by BED, updating beliefs and evaluating information gain in the high-dimensional network parameter space via a full Bayesian perspective (e.g., Monte Carlo methods) are often computationally infeasible. Recently, an automatic differentiable ensemble Kalman inversion (AD-EKI) approach was proposed by [56] to efficiently address the belief updating of high-dimensional network parameters for model discrepancies within the BED framework, building on the ensemble Kalman methods [57, 58] that have been actively studied in the past decade as an efficient derivative-free method for Bayesian inverse problems.

In this work, we assess the use of Wasserstein distance for the utility function of BED, in the presence of model discrepancy using the AD-EKI framework [56]. The model discrepancy is characterized by a trainable neural network, and a comprehensive comparison between Wasserstein distance and KL divergence is investigated in this work, for both low-dimensional physical parameters and high-dimensional neural network parameters. The key highlights of our work are summarized below:

- We investigate a limitation of using Wasserstein distance to construct the utility function in BED – when compared with an approximately uniform prior, its location dependence can induce false reward unrelated to information gain.
- We compare Wasserstein distance and KL divergence without model discrepancy. Starting from a uniform prior, Wasserstein distance tends to favor designs whose induced posteriors

place more mass near the boundary of the prior support. Though this effect is most pronounced only in the early stages, our experiments further show that such design preference often retains higher posterior uncertainty, thereby slowing down belief updating in subsequent stages of prior-based EIG methods.

- We extend the comparison to settings with model discrepancy, and show under actual utilities that KL's posterior tends to over-concentrate on incorrect regions, while Wasserstein designs preserve uncertainty around the true parameter and correct both belief and model more effectively. When switching to expected utilities, the performance gap narrows because the expected procedure introduces additional uncertainty, and the metric that retains more probability mass around the truth achieves faster updating and convergence.

This paper is organized as follows. Section 2 introduces the general formulation of BED with model discrepancy, using the Wasserstein distance to construct the utility function. Section 3 provides a comprehensive study of a classical BED problem to facilitate the comparison between the performances of Wasserstein distance and KL divergence. Section 4 concludes the paper.

2. Methodology

2.1. Bayesian experimental design

The Bayesian experimental design [30, 32, 33] provides a general framework to systematically seek the optimal design by solving the optimization problem:

$$\begin{aligned} \mathbf{d}^* &= \arg \max_{\mathbf{d} \in \mathcal{D}} \mathbb{E}[U(\boldsymbol{\theta}, \mathbf{y}, \mathbf{d})] \\ &= \arg \max_{\mathbf{d} \in \mathcal{D}} \int_{\mathbf{y}} \int_{\boldsymbol{\theta}} U(\boldsymbol{\theta}, \mathbf{y}, \mathbf{d}) p(\boldsymbol{\theta}, \mathbf{y} | \mathbf{d}) d\boldsymbol{\theta} d\mathbf{y}, \end{aligned} \quad (1)$$

where $\mathbf{y} \in \mathcal{Y} \subset \mathbb{R}^{d_y}$ is data from the experimental design $\mathbf{d} \in \mathcal{D} \subset \mathbb{R}^{d_d}$, $\boldsymbol{\theta} \in \Theta \subset \mathbb{R}^{d_{\theta}}$ denotes the target parameters, and U is the utility function taking the inputs of \mathbf{y} and $\boldsymbol{\theta}$ and returning a real value, which reflects the specific purpose of designing the experiment. The optimal design \mathbf{d}^* is obtained by maximizing the expected utility function $\mathbb{E}[U(\boldsymbol{\theta}, \mathbf{y}, \mathbf{d})]$ over the design space \mathcal{D} . The term $p(\boldsymbol{\theta}, \mathbf{y} | \mathbf{d})$ is the joint conditional distribution of data and parameters.

The utility function $U(\boldsymbol{\theta}, \mathbf{y}, \mathbf{d})$ can be regarded as the information gain obtained from the data \mathbf{y} for the corresponding design \mathbf{d} . A most common choice in Bayesian setting is the Kullback-Leibler (KL) divergence between the posterior and the prior distribution of parameters $\boldsymbol{\theta}$:

$$\begin{aligned} U(\boldsymbol{\theta}, \mathbf{y}, \mathbf{d}) &= D_{\text{KL}}(p(\boldsymbol{\theta} | \mathbf{y}, \mathbf{d}) \| p(\boldsymbol{\theta})) \\ &= \mathbb{E}_{\boldsymbol{\theta} | \mathbf{d}, \mathbf{y}} (\log p(\boldsymbol{\theta} | \mathbf{y}, \mathbf{d}) - \log p(\boldsymbol{\theta})) \\ &= \int_{\Theta} p(\boldsymbol{\theta} | \mathbf{y}, \mathbf{d}) \log \left(\frac{p(\boldsymbol{\theta} | \mathbf{y}, \mathbf{d})}{p(\boldsymbol{\theta})} \right) d\boldsymbol{\theta}, \end{aligned} \quad (2)$$

where $p(\boldsymbol{\theta} | \mathbf{y}, \mathbf{d})$ is the posterior distribution of $\boldsymbol{\theta}$ given a design \mathbf{d} and the data \mathbf{y} . Note that data \mathbf{y} could be either from the actual experimental measurement or the numerical model simulation. The use of KL divergence as the utility function leads to the definition of expected information gain

(EIG, [29]) that integrates the information gain over all possible predicted data:

$$\begin{aligned} \text{EIG}(\mathbf{d}) &= \mathbb{E}_{\mathbf{y}|\mathbf{d}}[D_{\text{KL}}(p(\boldsymbol{\theta}|\mathbf{y}, \mathbf{d})\|p(\boldsymbol{\theta}))] \\ &= \int_{\mathbf{y}} D_{\text{KL}}(p(\boldsymbol{\theta}|\mathbf{y}, \mathbf{d})\|p(\boldsymbol{\theta}))p(\mathbf{y}|\mathbf{d})d\mathbf{y}, \end{aligned} \quad (3)$$

where $p(\mathbf{y}|\mathbf{d}) := \mathbb{E}_{\boldsymbol{\theta}}[p(\mathbf{y}|\boldsymbol{\theta}, \mathbf{d})]$ is the distribution of the predicted data among all possible parameter values given a certain design.

2.2. Wasserstein distance criteria

Recent work [40] has proposed using the Wasserstein distance, which is also a metric to quantify divergence between two distributions, as the utility function in BED. Let ρ_0 and ρ_1 be two probability measures on a domain $\Omega \subset \mathbb{R}^d$. The Wasserstein- p distance, with $p \geq 1$, is defined as

$$W_p^p(\rho_0, \rho_1) = \inf_{\gamma \in \Gamma(\rho_0, \rho_1)} \int_{\Omega \times \Omega} \|x - y\|^p d\gamma(x, y), \quad (4)$$

where $\Gamma(\rho_0, \rho_1)$ denotes the set of all couplings with marginals ρ_0 and ρ_1 . In this study, we focus on $p = 2$ and $p = 1$, corresponding to the W_2 and W_1 distances, respectively. For Gaussian measures $\rho_0 = \mathcal{N}(m_0, C_0)$ and $\rho_1 = \mathcal{N}(m_1, C_1)$, the squared W_2 distance admits the well-known closed-form expression [59]:

$$W_2^2(\rho_0, \rho_1) = \|m_0 - m_1\|_2^2 + \text{tr} \left(C_0 + C_1 - 2 \left(C_1^{1/2} C_0 C_1^{1/2} \right)^{1/2} \right), \quad (5)$$

where $\text{tr}(\cdot)$ denotes the trace operator. The W_1 distance between Gaussian measures does not generally admit a simple matrix-based closed form, except in one dimension it reduces to the L^1 distance between their means.

In most practical scenarios of BED, the prior and posterior distributions of the physical parameters are non-Gaussian due to nonlinear forward models and non-Gaussian priors. In such cases, the Gaussian closed form (5) is no longer applicable, and the computation of W_2 or W_1 must rely on numerical methods for optimal transport.

In [40], the authors address the non-Gaussian setting by solving the Monge–Ampère PDE associated with the optimal transport map. Specifically, they represent the convex potential function via a radial basis function (RBF) expansion and employ the Kansa collocation method to solve the PDE under convexity constraints. Once the optimal map is obtained, the Wasserstein distance is computed by numerical integration over the parameter domain.

In the present work, to facilitate automatic differentiation, we adopt a simpler and more flexible computational strategy based on the discrete optimal transport formulation. Let $\mu = \sum_{i=1}^n a_i \delta_{x_i}$ and $\nu = \sum_{j=1}^m b_j \delta_{y_j}$ be empirical measures of the prior and posterior, with $a_i, b_j > 0$ and $\sum_i a_i = \sum_j b_j = 1$. We approximate W_2 using the entropic-regularized discrete optimal transport formulation

$$\text{OT}_{\varepsilon}^{(2)}(\mu, \nu) = \min_{\gamma \in \mathbb{R}_+^{n \times m}} \langle C, \gamma \rangle + \varepsilon D_{\text{KL}}(\gamma \| ab^\top) \quad \text{s.t.} \quad \gamma \mathbf{1}_m = a, \quad \gamma^\top \mathbf{1}_n = b, \quad (6)$$

where $C_{ij} = \|x_i - y_j\|^2$ is the quadratic ground cost, $\langle C, \gamma \rangle = \sum_{ij} C_{ij} \gamma_{ij}$, and $D_{\text{KL}}(\gamma \| ab^\top) = \sum_{ij} \gamma_{ij} \log(\gamma_{ij}/(a_i b_j))$. The regularization parameter $\varepsilon > 0$ smooths the transport plan and enables

fast convergence of the Sinkhorn iterations implemented in `ott-jax`. In practice, we form the empirical weight vectors a and b from normalized histograms of the prior and posterior samples, apply a small jitter to avoid zero entries, and solve (6) with the `LinearProblem` and `Sinkhorn` solver in `ott-jax`. The approximate Wasserstein-2 distance is then obtained as

$$\widehat{W}_2(\mu, \nu) = \sqrt{\text{OT}_\varepsilon^{(2)}(\mu, \nu)}, \quad (7)$$

where $\text{OT}_\varepsilon^{(2)}(\mu, \nu)$ is returned by the solver as the regularized OT cost. We note that, due to entropic regularization, \widehat{W}_2 is a biased approximation to the unregularized W_2 , but offers substantial computational speedup, GPU scalability, and automatic differentiation, which are critical in repeated evaluations of EIG and gradient-based design search of BED.

2.3. False reward of Wasserstein distance

Although Wasserstein distance admits several advantages as a utility function in BED, it might mislead design choices. The underlying reason is that, even when two designs yield posteriors with the same shape but centered at different locations, the one located nearer to the boundary of the prior's bounded support will register a larger Wasserstein distance, purely as a boundary effect. This increase in distance does not necessarily reflect a true gain in information, but rather arises from the location-dependent nature of the Wasserstein metric. When such cases occur, the Wasserstein utility may favor a suboptimal design that produces a posterior with greater uncertainty.

This location effect is further compounded when the posterior is more diffuse. Although such posteriors may cover the true value, their mass is spread more broadly, and most of it may still be located far from the true value. Moving prior mass to these far-away regions can incur a larger transport cost than moving it to the true value, which can result in a higher Wasserstein distance despite the posterior being less informative.

To illustrate this location-dependent effect, consider a one-dimensional parameter space with a uniform prior on the support $[-A, A]$. We examine three posterior distributions:

- a delta distribution at $0, \delta(0)$;
- two symmetric delta distributions, $0.5\delta(-\Delta x) + 0.5\delta(\Delta x)$;
- a shifted symmetric delta distribution, $0.5\delta(-\Delta x + \mu) + 0.5\delta(\Delta x + \mu)$, with $\Delta x < A$ and $\Delta x + \mu < A$.

These three distributions can be regarded as a single delta distribution to be evenly separated and then moved together. We give the analytical solutions of the Wasserstein-2 distance between them and a uniform prior, respectively, to show that this false reward does happen.

The Wasserstein-2 distances of these three distributions from the uniform prior are:

$$W_2^{(1)} = A/\sqrt{3}, \quad W_2^{(2)} = \sqrt{\Delta x^2 - A\Delta x + A^2/3}, \quad W_2^{(3)} = \sqrt{\mu^2 + \Delta x^2 - A\Delta x + A^2/3}, \quad (8)$$

and detailed derivations can be found in Appendix A.

Intuitively, a delta distribution at the center of the support exhibits greater discrepancy from the uniform prior than two equally weighted deltas symmetrically located within the support. Consequently, $W_2^{(1)} \geq W_2^{(2)}$, with equality only when $\Delta x = 0$ or $\Delta x = A$. However, when the

symmetric pair is shifted toward the boundary, its corresponding Wasserstein distance will increase, i.e., $W_2^{(3)} \geq W_2^{(2)}$. For sufficiently large μ , specifically when $\mu^2 > A\Delta x - \Delta x^2$, we have $W_2^{(3)} = \sqrt{\mu^2 + \Delta x^2 - A\Delta x + A^2/3} > W_2^{(1)} = A/\sqrt{3}$. In this regime, the Wasserstein distance for the two-point configuration exceeds that for the single point mass.

This example shows that a more diffuse distribution, if shifted toward the boundaries, can be assigned a larger Wasserstein distance from the uniform prior than a concentrated distribution at the center. In other words, the location-dependent property of Wasserstein distance can make a shifted, diffuse distribution appear to carry more information relative to the prior, even when it does not. Once the symmetric delta distribution is shifted toward the boundaries, some prior mass from the opposite side must be transported across the entire domain to reach the posterior's concentration region. This additional transport inflates the distance metric and creates a false information gain in the design context.

It is noteworthy that for these examples, the KL divergence from the uniform prior remains unchanged regardless of the shift, underscoring a key difference between Wasserstein distance and KL divergence as measures of distributional discrepancy.

In summary, this simplified case provides insight into why Wasserstein-based design choices can diverge from those based on KL divergence. A diffuse posterior shifted toward the boundary may appear more different from the prior in terms of Wasserstein distance than a concentrated posterior at the center, despite being no more informative. This location-dependent property can assign high utility values to certain posteriors, leading to design selections that differ from those favored by KL divergence. While the posteriors here are chosen arbitrarily for illustration, more design-relevant examples are presented in Section 3.

2.4. Correction strategy under model discrepancy

We not only compare the performance between classical KL divergence and Wasserstein distance in the traditional setting (i.e., exact model), but also in the presence of model discrepancy. When there is no model discrepancy, we follow the standard sequential BED framework with a greedy strategy in each experiment as described in Section 2.1. However, model discrepancy is ubiquitous in real-world applications, posing challenges to both forward and inverse problems, not to mention active learning and BED. Under model discrepancy scenarios, we build on the framework in [56] and additionally specify a re-update process to improve effectiveness for the expected utilities. Although this framework has proved effective in structural error cases with data-driven methods, we consider only parametric error in this work, as our focus is to compare different metrics rather than dealing with complicated structural discrepancies. Also, the parametric error will make it easier to compare the performance gap between different metrics.

Specifically, to define the model discrepancy, the true system is written in general form

$$\mathbf{y} = \mathcal{G}^\dagger(\boldsymbol{\theta}_G; \mathbf{d}) + \boldsymbol{\epsilon}, \quad \boldsymbol{\epsilon} \sim \mathcal{N}(\mathbf{0}, \Sigma^2), \quad (9)$$

while the incorrect model is

$$\mathbf{y} = \mathcal{G}(\boldsymbol{\theta}_G, \boldsymbol{\theta}_E; \mathbf{d}), \quad (10)$$

where $\boldsymbol{\theta}_G$ represents the original physical parameter, $\boldsymbol{\theta}_E$ represents the error parameter, and $\boldsymbol{\epsilon}$ represents the zero-mean Gaussian noise with covariance matrix Σ^2 . Note that the system \mathcal{G}^\dagger and model \mathcal{G} may also serve as the right-hand-side of dynamic systems, and in that case design \mathbf{d} usually appear in the additional measuring operator, rather than the input of dynamic systems. To calibrate

the model discrepancy, we seek to optimize the error parameter $\theta_{\mathcal{E}}$ such that the model \mathcal{G} could approximate the system \mathcal{G}^\dagger .

In the context of BED, this framework determines optimal designs for physical parameters $\theta_{\mathcal{G}}$ and error parameters $\theta_{\mathcal{E}}$, respectively. The purpose of separating these two types of parameters rather than jointly seeking designs and updating is to avoid the high-dimensional joint parameter space $\{\theta_{\mathcal{G}}, \theta_{\mathcal{E}}\}$, especially when using a neural network to calibrate structural model discrepancy. At each stage in the sequential process, for relatively low-dimensional physical parameters, we retain standard BED methods to allow arbitrary distributions. For high-dimensional error parameters, we (1) assume Gaussian distributions and follow the automatic differential ensemble Kalman inversion (AD-EKI) framework to find designs, (2) use a gradient-based method to update their deterministic values. These two steps are repeated in each stage. The updated model benefits the updating in later stages, and the updated belief allows more effective model correction.

At each stage of sequential BED, the optimal design for physical parameters is determined using standard BED:

$$\mathbf{d}_{\mathcal{G}}^* = \arg \max_{\mathbf{d} \in \mathcal{D}} \mathbb{E}[U(p(\theta_{\mathcal{G}}|\mathbf{y}; \theta_{\mathcal{E}})||p(\theta_{\mathcal{G}}))], \quad (11)$$

where the posterior distribution of $\theta_{\mathcal{G}}$ from the previous stage serves as the prior distribution $p(\theta_{\mathcal{G}})$ for the current stage. The utility function U could either be the KL divergence or the Wasserstein distance. Considering that $\theta_{\mathcal{G}}$ is often low-dimensional, standard BED methods can be employed to solve the optimization problem in Eq. (11). With the optimal design $\mathbf{d}_{\mathcal{G}}^*$, the corresponding data $\mathbf{y}_{\mathcal{G}}$ is then used to update the belief of physical parameters by the Bayesian theorem conditioned on the current network coefficients θ_{NN} :

$$p(\theta_{\mathcal{G}}|\mathbf{y}_{\mathcal{G}}, \mathbf{d}_{\mathcal{G}}^*; \theta_{\mathcal{E}}) = \frac{p(\mathbf{y}_{\mathcal{G}}|\theta_{\mathcal{G}}, \mathbf{d}_{\mathcal{G}}^*; \theta_{\mathcal{E}})p(\theta_{\mathcal{G}})}{p(\mathbf{y}_{\mathcal{G}}|\mathbf{d}_{\mathcal{G}}^*; \theta_{\mathcal{E}})}, \quad (12)$$

which also provides the MAP estimation of physical parameters $\theta_{\mathcal{G}}^*$:

$$\theta_{\mathcal{G}}^* = \arg \max_{\theta_{\mathcal{G}}} \{p(\theta_{\mathcal{G}}|\mathbf{y}_{\mathcal{G}}, \mathbf{d}_{\mathcal{G}}^*; \theta_{\mathcal{E}})\}. \quad (13)$$

On the other hand, the optimal design for neural network parameters is found by BED with the ensemble-based utility function:

$$\begin{aligned} \mathbf{d}_{\mathcal{E}}^* &= \arg \max_{\mathbf{d} \in \mathcal{D}} \mathbb{E}[U(p(\theta_{\mathcal{E}}|\mathbf{y}; \theta_{\mathcal{G}}^*)||p(\theta_{\mathcal{E}}))], \\ &= \arg \max_{\mathbf{d} \in \mathcal{D}} \mathbb{E}[U(\{\tilde{\theta}_{\mathcal{E}}^{(j)}\}_{j=1}^J || \{\theta_{\mathcal{E}}^{(j)}\}_{j=1}^J)] \end{aligned} \quad (14)$$

where $\{\tilde{\theta}_{\mathcal{E}}^{(j)}\}_{j=1}^J$ and $\{\theta_{\mathcal{E}}^{(j)}\}_{j=1}^J$ represent the updated and initial ensemble in EKI, respectively. The metric choice for U aligns with that in Eq. (11). No matter what kind of metric is chosen, the AD-EKI introduced in [56] allows direct acquisition of the gradient of expected utility to design. At each stage of the sequential BED, we assume a Gaussian prior over the error parameters centered at their current value to enable ensemble update for EKI. Once the design $\mathbf{d}_{\mathcal{E}}^*$ is determined, the resulting data $\mathbf{y}_{\mathcal{E}}$ is then used to update the network coefficients via standard gradient-based optimization:

$$\theta_{\mathcal{E}}^* = \arg \max_{\theta_{\mathcal{E}}} p(\mathbf{y}_{\mathcal{E}}|\theta_{\mathcal{G}}^*, \mathbf{d}_{\mathcal{E}}^*, \theta_{\mathcal{E}}). \quad (15)$$

At each stage, we immediately use the updated model ($\boldsymbol{\theta}_{\mathcal{E}}^*$) and the previously collected data for physical parameters, $\mathbf{y}_{\mathcal{G}}$, to refine the belief of the physical parameter $\boldsymbol{\theta}_{\mathcal{G}}$. Unlike the standard sequential BED approach, which propagates the posterior from the previous stage as the new prior, we adopt a re-update strategy that incorporates all accumulated data into the posterior update from the initial prior distribution. Specifically, the physical parameter posterior is recomputed as:

$$p(\boldsymbol{\theta}_{\mathcal{G}}|\mathbf{Y}_{\mathcal{G}}, \mathbf{D}_{\mathcal{G}}; \boldsymbol{\theta}_{\mathcal{E}}^*) = \frac{p(\mathbf{Y}_{\mathcal{G}}|\boldsymbol{\theta}_{\mathcal{G}}, \mathbf{D}_{\mathcal{G}}; \boldsymbol{\theta}_{\mathcal{E}}^*)p(\boldsymbol{\theta}_{\mathcal{G}})}{p(\mathbf{Y}_{\mathcal{G}}|\mathbf{D}_{\mathcal{G}}; \boldsymbol{\theta}_{\mathcal{E}}^*)}, \quad (16)$$

where $\mathbf{D}_{\mathcal{G}} = \{\mathbf{d}_{\mathcal{G}}^n, \mathbf{d}_{\mathcal{G}}^{n-1}, \dots, \mathbf{d}_{\mathcal{G}}^1\}$ and $\mathbf{Y}_{\mathcal{G}} = \{\mathbf{y}_{\mathcal{G}}^n, \mathbf{y}_{\mathcal{G}}^{n-1}, \dots, \mathbf{y}_{\mathcal{G}}^1\}$ denote the sequence of historical designs and corresponding observations, and $p(\boldsymbol{\theta}_{\mathcal{G}})$ is the original prior, which may be uniform.

This re-update strategy helps correct the accumulating effect of early-stage model errors. When the model is not yet well corrected in early stages, posteriors updated via incorrect model may inherit inaccuracies from the model discrepancy. In sequential setting, by re-initializing the inference of $\boldsymbol{\theta}_{\mathcal{G}}$ from the original prior and incorporating all accumulated data with an improved model, we effectively remove the influence of previously biased posteriors and instead rely more directly on the observed data and the current, better-corrected model.

Notice that the alternating re-update and model-correction steps require no additional experiments or data acquisition. They are performed using accumulated data, solely by post computation. When computational cost is small relative to measurement cost, the procedure can be repeated multiple times. Conceptually, this alternating post-process scheme can progressively improve the posterior belief over physical parameters and the corrected model, and may converge to a stationary point. The attained solution is not necessarily globally optimal: its accuracy is constrained by the measurement noise in the available data and by limitations to the alternating-update framework. Formal convergence criteria and dedicated denoising or regularization strategies remain topics for future work.

3. Numerical Results

In this work, we mainly consider a classical source inversion problem in BED community [60, 61, 40, 56]. This problem assumes a plume source located at an unknown position in a two-dimensional spatial domain, governed by certain PDE (i.e., combinations of convection, diffusion, and reaction). For each experimental design, a scalar concentration value can be measured at a certain location, and the goal is to infer the probability distribution of the source location based on the measurement, with a series of optimally designed measurement locations. Sometimes other properties of the system, e.g., source strength [62] and convective velocity [45], are also assumed to be unknown and left for inference.

In this work, we aim to investigate the BED performance based on the expected Wasserstein metric and compare it with the classical expected KL divergence. We first study the performance comparison in the setting without model discrepancy and then extend to a more challenging setting where model discrepancy is non-negligible and is characterized by a trained neural network.

The key motivations and conclusions of the numerical results are summarized below:

- We first study a single-stage two-dimensional toy source inversion example to demonstrate that Wasserstein distances can produce false increases in reward when the posterior mass is shifted toward the boundary of the prior support. This location-driven effect arises from transport geometry rather than information gain, and can mislead the design choice.

- We then compare KL divergence and Wasserstein distances using a convection–diffusion plume inversion example without model discrepancy under a sequential BED setting. With actual utilities, KL leads to posteriors that converge more rapidly to the true source location, while Wasserstein metrics can be misled by location bias with a non-informative prior and also yield more uncertainties in posteriors at subsequent stages of sequential BED. With expected utilities, the performance gap narrows because the expectation introduces additional uncertainty to both KL- and Wasserstein-based utilities. In this setting, KL still yields superior designs in most cases.
- We further study the performance comparison under model discrepancy. Interestingly, the smaller uncertainties in the posteriors produced by the KL-based utility become a disadvantage. With actual utilities, KL starts to lead biased posteriors and thus slows down the model correction, while results via Wasserstein-based utility retain more uncertainties in posteriors and thus avoid a rapid convergence to biased estimation of source location and incorrect model discrepancy. With expected utilities, the performance gap also narrows. In this setting, Wasserstein yields superior designs in most cases by retaining greater probability mass near the true value and provides a faster correction of model discrepancy.

3.1. A toy example of 2-D inverse problem

We first consider a simplified but general two-dimensional toy example in a single-step design to illustrate the false reward effect of Wasserstein distance in BED. This example aims to show how the Wasserstein distance between posterior and prior can misleadingly increase with certain design choices, even when information gain does not actually improve.

3.1.1. Setup

We begin with a simplified toy example formulated within the source inversion framework. This example involves two key modeling assumptions. First, rather than specifying a single governing equation, we consider a broad class of systems in which the observation is represented as a function of the relative position between the observation point and the source. Specifically, the observation model takes the form

$$y = f(\mathbf{z} - \boldsymbol{\theta}), \quad (17)$$

where $\mathbf{z} \in \mathbb{R}^2$ denotes the sensor(observation) location, $\boldsymbol{\theta} \in \mathbb{R}^2$ is the unknown source location, and $y \in \mathbb{R}$ is the observed scalar concentration. The function f is assumed to be isotropic and monotonically decreasing with respect to the Euclidean distance $\|\mathbf{z} - \boldsymbol{\theta}\|$. This assumption defines a family of models that includes many commonly used physical processes with a decaying source, such as diffusive or dispersive transport. For example, admissible forms of f include

$$y = -\|\mathbf{z} - \boldsymbol{\theta}\| + B \quad \text{or} \quad y = \exp(-\|\mathbf{z} - \boldsymbol{\theta}\|^2), \quad (18)$$

both of which are radially symmetric and consistent with the physical intuition that concentration decreases with increasing distance from the source.

Second, we assume that the measurement is noise-free, which makes this a toy example. As a consequence, the likelihood function becomes a Dirac delta distribution: for any candidate parameter $\boldsymbol{\theta}$, the likelihood equals 1 if the model prediction exactly matches the observation, and 0 otherwise. Under this assumption, a single measurement induces a posterior distribution over the

parameter space in the shape of a circular ring. The ring is centered at the measurement location z , and the true source θ lies on its circumference. Due to isotropic assumption, the posterior has zero thickness and behaves like a delta distribution over the circle in \mathbb{R}^2 .

For numerical testing, we define the spatial domain as the square region $[0, 3]^2$, which bounds both the sensor deployment region and the parameter space. The true source location is set at $\theta = \{0.9, 1.2\}$, and the prior distribution is assumed to be uniform over the same domain, representing non-informative beliefs about the source position.

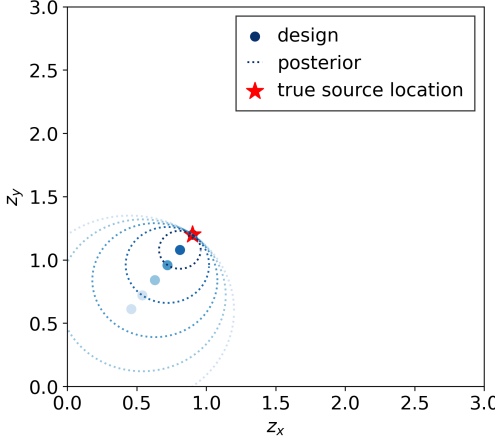
We select several candidate sensor locations and calculate corresponding posteriors and their KL divergence /Wasserstein distance against prior. Specifically, these sensor locates along the straight line connecting the source location and the lower-left corner of the domain. Our goal is to analyze how a single measurement affects the posterior distribution and to identify which candidate measurement location provides the greatest actual information gain.

3.1.2. Results

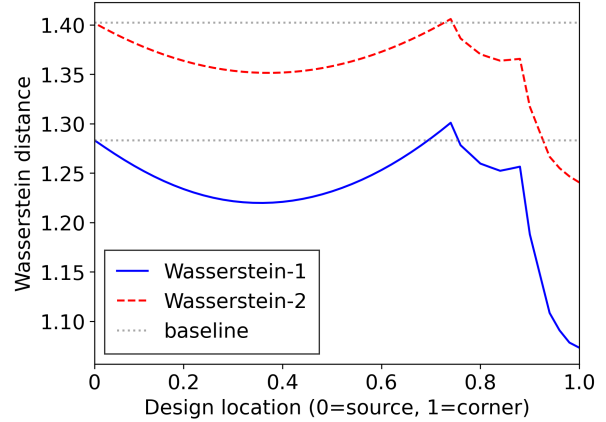
Figure 1a illustrates the overall setup. As the design point moves further from the source location toward the boundary of the domain, the posterior circles grow in radius, eventually touching or exceeding the boundary. If the posterior mass extends beyond the parameter support, it would be truncated in standard Bayesian computations.

Figure 1b shows how the Wasserstein distance between posterior and prior varies with the design location. When the design is within approximately 40% of the diagonal distance (along its way from source to corner), the Wasserstein distance decreases. This agrees with intuition: a posterior highly concentrated around the true source (a delta distribution) should be more informative than a circular posterior with probability spread in multiple directions. Beyond this range, however, the Wasserstein distance begins to increase. The rise is not due to reduced uncertainty, but rather to transport geometry: moving prior mass from the far upper-right region of the support to a posterior increasingly concentrated near the lower-left incurs a large relocation cost. We refer to this behavior as a false increase in reward, since it exaggerates the apparent informativeness of the design without reflecting actual information gain. Notably, around 70% along the diagonal, the Wasserstein distance associated with a circular posterior can exceed that of the delta posterior centered at the truth, incorrectly suggesting that such designs are more informative. As the design approaches the boundary, the posterior is truncated by the support and the Wasserstein distance decreases again, creating a local maximum. Such a maximum of information gain indicates that if Wasserstein distance were used directly as an information metric in BED, this would incorrectly suggest that these designs yield greater information, even though they actually produce misleading posteriors.

This example highlights the potential limitation of using Wasserstein distance as information gain: its value depends not only on posterior uncertainty but also on the relative spatial position of posterior mass with respect to the prior support. Such spatial effects can therefore mislead design selection. A simple mitigation is to enlarge the support domain used to define the prior, which effectively shifts the true parameter away from the boundary and reduces the chance of encountering false increases, at the cost of increasing computational burden.



(a) Design and posterior



(b) Reward vs. design

Figure 1: Illustration of design and associated reward. Panel (a) Design and posterior: each filled circle denotes a design point, and the dotted circle of the same color indicates its corresponding posterior distribution. The red star marks the true source location. Panel (b) Reward vs. design: Wasserstein-1 and Wasserstein-2 distances are plotted as functions of the design location, normalized so that 0 corresponds to the source location and 1 to the domain corner. The grey dotted line shows the baseline.

3.2. An inverse problem of convection-diffusion equation without model discrepancy

3.2.1. Setup

To compare the KL divergence and Wasserstein distance in a more realistic case, we study the source inversion problem of a contaminant in the convection-diffusion field, which is a classical test example in BED and has been previously studied in [62, 45]. More specifically, the contaminant concentration \mathbf{u} at two-dimensional spatial location $\mathbf{z} = \{z_x, z_y\}$ and time t is governed by the following equation:

$$\frac{\partial \mathbf{u}(\mathbf{z}, t; \boldsymbol{\theta})}{\partial t} = D \nabla^2 \mathbf{u} - \mathbf{v}(t) \cdot \nabla \mathbf{u} + S(\mathbf{z}, t; \boldsymbol{\theta}), \quad \mathbf{z} \in [z_L, z_R]^2, \quad t > 0, \quad (19)$$

where D is the diffusion coefficient assumed to be known with a true value of 1, $\mathbf{v} = \{v_x, v_y\} \subseteq \mathbb{R}^2$ is a time-dependent convection velocity assumed to be known with true value of $v_x = v_y = 50t$, S denotes the source term with some parameters $\boldsymbol{\theta}$. In this work, the true system has an exponentially decay source term in the following form with the parameters $\boldsymbol{\theta} = \{\theta_x, \theta_y, \theta_h, \theta_s\} \in \mathbb{R}^4$:

$$S(\mathbf{z}, t; \boldsymbol{\theta}) = \frac{\theta_s}{2\pi\theta_h^2} \exp\left(-\frac{(\theta_x - z_x)^2 + (\theta_y - z_y)^2}{2\theta_h^2}\right), \quad (20)$$

where θ_x and θ_y denote the source location, θ_h and θ_s represent the source width and source strength. The initial condition is $\mathbf{u}(\mathbf{z}, 0; \boldsymbol{\theta}) = \mathbf{0}$, and a homogeneous Neumann boundary condition is imposed for all sides of the square domain.

Note that in this work, the inversion is performed over a finite-dimensional parameter set $\boldsymbol{\theta}$ which governs the source term (e.g., source location, width, and strength). The state variable \mathbf{u} is not directly inferred but is obtained by solving the governing PDE given $\boldsymbol{\theta}$.

In all numerical examples, the physics-based unknown parameters $\boldsymbol{\theta}_G$ are the location $\{\theta_x, \theta_y\}$ of the source. The parameter space is set as $[0, 1]^2$. The true value varies in different cases:

Case	θ_x	θ_y
1 & 2 & 4	0.3	0.4
3	0.4	0.4
5	0.1	0.1

Table 1: Values of θ_x and θ_y for different cases. Case 5 is presented in the appendix.

The true value of other parameters in the source term is set as $\theta_s = 2$ and $\theta_h = 0.05$. The PDE is numerically solved on $[-2, 3]^2$, which is larger than the parameter space, to avoid any boundary effects.

The design $\mathbf{d} = \{d_x, d_y\}$ in this problem refers to the spatial coordinate to measure the concentration value. More specifically, each design involves measuring just one point in the domain. The temporal coordinates of the measurement are set as $0.05 + n \times 0.005$ time units, where n is the stage number ($n = 1, 2, \dots$). The design searching area is set as $[0, 1]^2$, which happens to be the same as the parameter space. Measurements contain a Gaussian noise $y = \mathbf{u}(\mathbf{d}) + \epsilon$, $\epsilon \sim \mathcal{N}(0, 0.05^2)$.

3.2.2. Case 1: Actual information gain

We conduct a six-stage sequential BED using three utility functions: KL divergence, Wasserstein-1 (W_1), and Wasserstein-2 (W_2). In this section, designs are optimized with the actual utility computed from the observed data at each step, rather than the expected utility; results based on expected utility are presented in the next section. The purpose of using actual utility in this section is to clearly reveal how each metric influences the design selection process and the resulting posterior distributions. This choice is potentially reasonable in scenarios where (i) a small preliminary measurement budget allows one to obtain actual rewards at a handful of locations and then extrapolate to higher-reward designs for subsequent measurements, or (ii) multi-fidelity sensing is available, so that low-precision probes can identify promising design points before committing high-precision measurements.

Figure 2 presents the evolution of the posterior across six stages. After the first measurement, the design chosen under KL divergence yields a posterior that is tightly centered near the true parameter with low uncertainty. By contrast, the designs selected by W_1 and W_2 tend to lie closer to the boundary of the support; their posteriors still cover the truth but place substantial probability mass away from it. This reproduces the conclusion of the previous section: the location-driven false reward effect causes Wasserstein-based utilities to prefer suboptimal designs when used directly as information metrics. And this bias degrades the performance of the Wasserstein distance.

We further look into some quantitative metrics to evaluate the posterior distribution of the source location $\{\theta_x, \theta_y\}$. We define the distance between the MAP point $\theta_{\mathcal{G}}^* = \{\theta_x^*, \theta_y^*\}$ and the true value $\theta_{\mathcal{G}}^\dagger = \{\theta_x^\dagger, \theta_y^\dagger\}$ in each stage:

$$D = \|\theta_{\mathcal{G}}^* - \theta_{\mathcal{G}}^\dagger\|_2 = \sqrt{(\theta_x^* - \theta_x^\dagger)^2 + (\theta_y^* - \theta_y^\dagger)^2}, \quad (21)$$

and the magnitude of uncertainty:

$$\sigma_{\text{eq}} = \sqrt[4]{\lambda_1 \lambda_2}. \quad (22)$$

where λ_1 and λ_2 are the eigenvalues of the posterior covariance matrix. Corresponding results are presented in Fig. 3. The least uncertainty given by KL at stage 1 further confirms its better performance. The reason for the nearly the same uncertainty starting from stage 2 is that two

data points are sufficient to constrain the two-dimensional unknown parameter when using actual information gain.

We also observe that the W_1 - and W_2 -selected designs differ slightly, as do the resulting posterior shapes. A plausible explanation is their different behavior to boundary-induced truncation. In the previous example in Section 3.1, the two metrics behaved similarly because the posteriors consisted of delta masses. By contrast, in this case, the posterior decays smoothly outside the circular shape, so truncation induces more intricate (and metric-dependent) behavior.

Notice we are using a greedy strategy at each stage. The difference between the KL divergence and the Wasserstein distance in long-term or accumulated reward is left for future work.

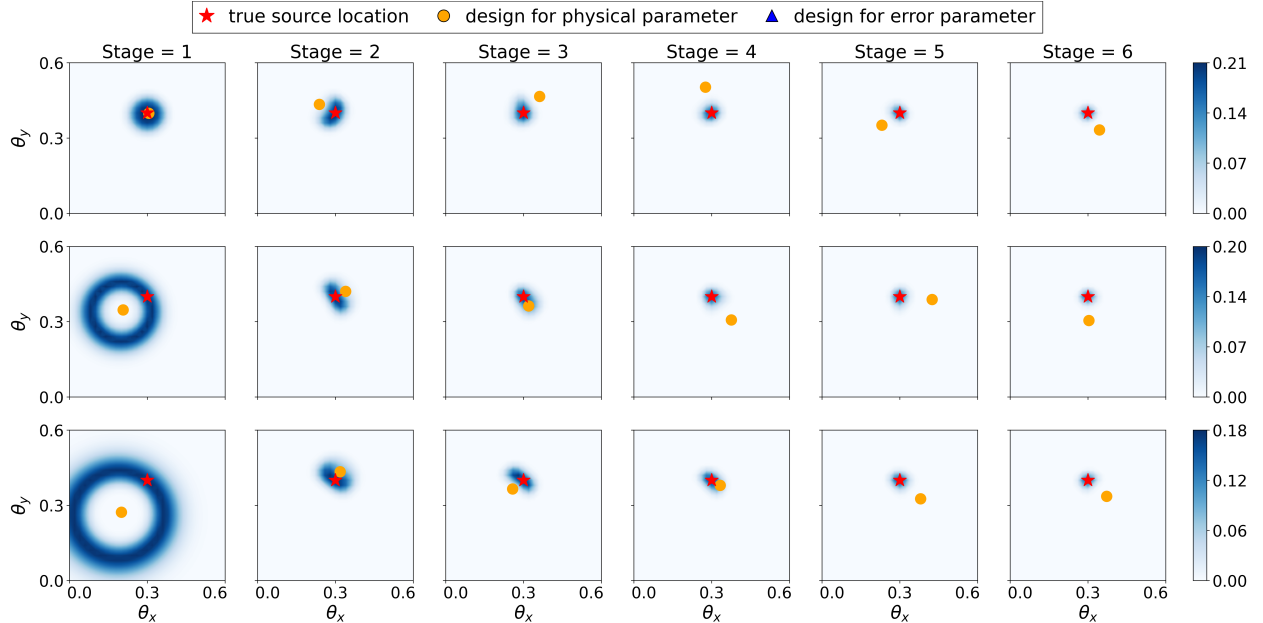


Figure 2: Without error (case 1), using actual information gain: posterior. From top to bottom: KL, W_2 , W_1 . The parameter space is set as $[0, 1]^2$ but zoomed in as $[0, 0.6]^2$. This holds for all the remaining posterior figures.

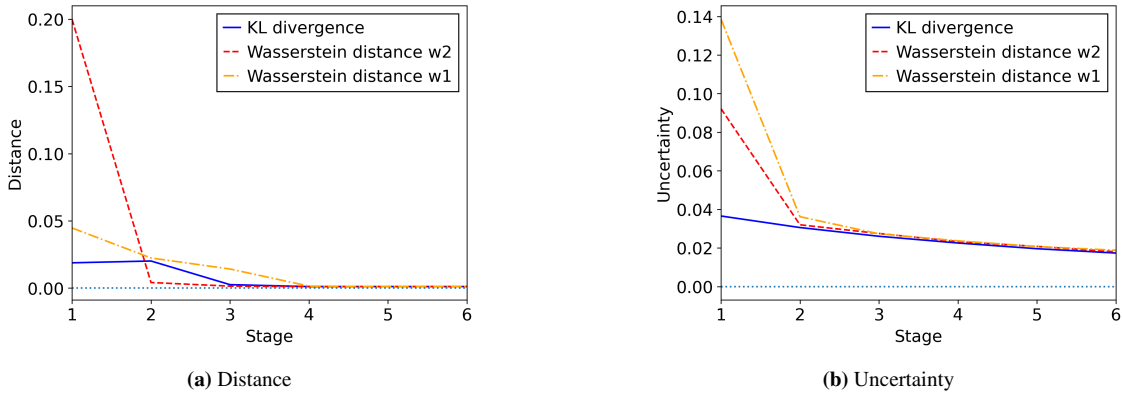


Figure 3: Distance and uncertainty evolution.

3.2.3. Case 2: Expected information gain

We now perform a six-stage sequential BED experiment using expected utility functions. An expected utility formulation corresponds to the practical scenario where no additional measurement

budget is available, and design selection must rely entirely on the predictive capability of the current model. In this setting, candidate measurement outcomes are simulated from the forward model and used to compute the expected information gain. This substantially reduces the need for real measurements but increases computational cost.

Figure 4 presents the reward map of different expected utilities at stage 1, depicting the contour of expected utility values across various design points. The reward map of expected KL divergence (Fig.4a) closely resembles Figure 10 in [62], where a similar case setup was used, indicating the reliability of the numerical results. Overall, the reward map of the expected Wasserstein distance is largely similar to that of the expected KL divergence, indicating that the expected Wasserstein distance is also suitable as a BED utility function. However, the locations of the extrema exhibit certain differences. The design points that yield the highest expected Wasserstein distance are located near those of expected KL divergence, suggesting that Wasserstein distance is a potential candidate for utility function, similar to KL divergence. However, a slight difference remains: the optimal design point based on expected Wasserstein distance lies slightly closer to the boundary compared to that of expected KL divergence, as more clearly illustrated in the first stage of Fig.5. This reflects the same false reward effect discussed in the previous section.

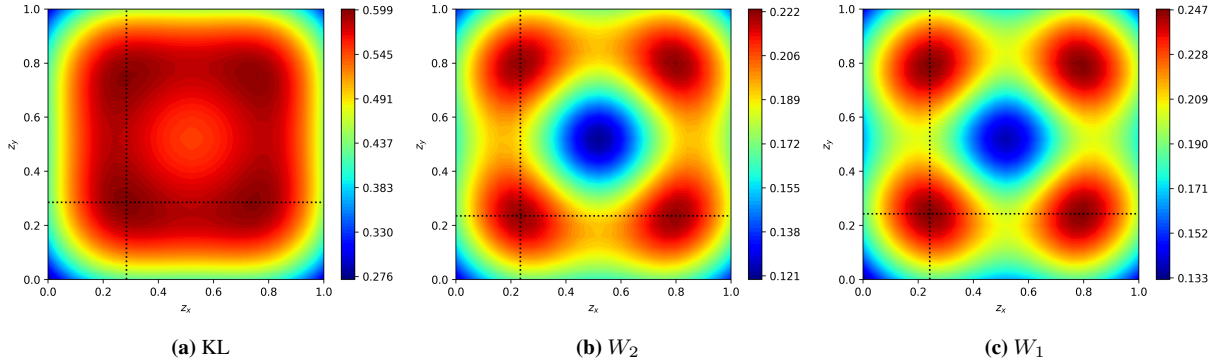


Figure 4: Reward map with no model discrepancy at stage 1. The black dotted lines indicate the z_x and z_y coordinates of the global maximizer.

Figure 5 shows the evolution of the posterior distributions over six stages. In stage 1, both W_1 and W_2 select designs that lie closer to the boundary of the domain compared to the KL divergence, resulting in more diffuse posteriors. Because these early-stage posteriors, which serve as priors for subsequent stages, retain substantial probability mass away from the true parameter, the following design choices become less effective at quickly eliminating uncertainty. As a result, the posteriors of W_1 and W_2 exhibit higher dispersion than those of KL even in the later stages. This inferior performance of Wasserstein distance is further confirmed by the uncertainty results in Fig. 6. In other words, the uncertainty in the posterior induced by the Wasserstein-based design requires one additional measurement to converge to the same level as that induced by the KL-based design.

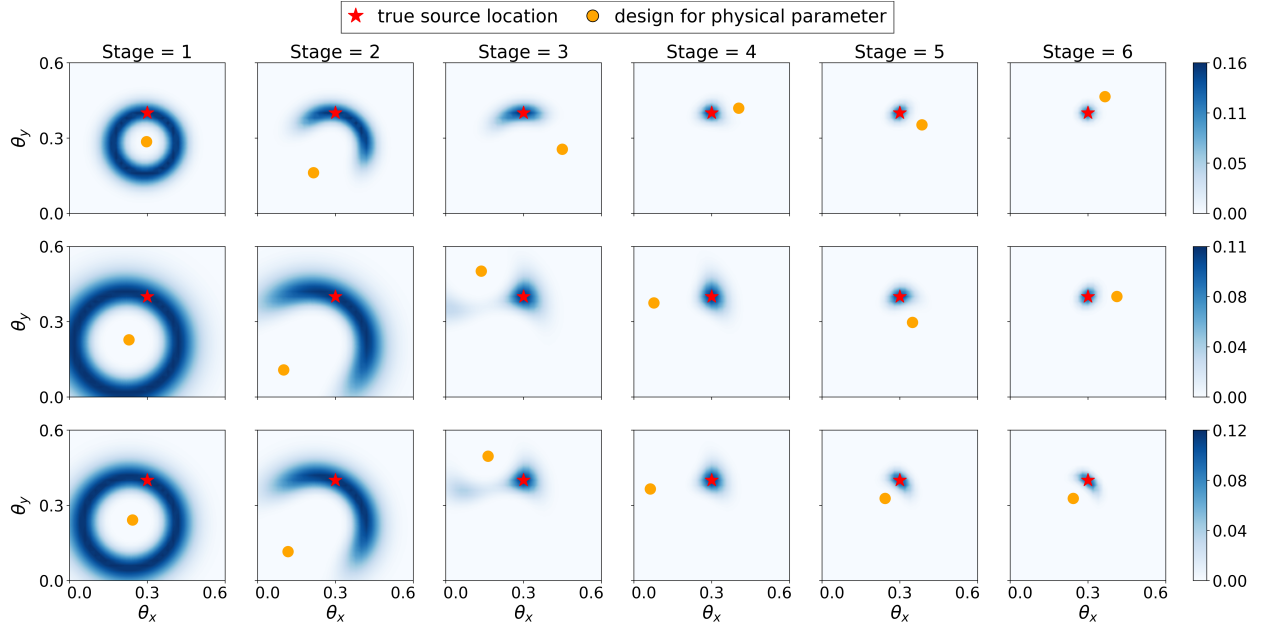


Figure 5: Without error (case 2), using expected information gain: posterior. From top to bottom: KL, W_2 , W_1 .

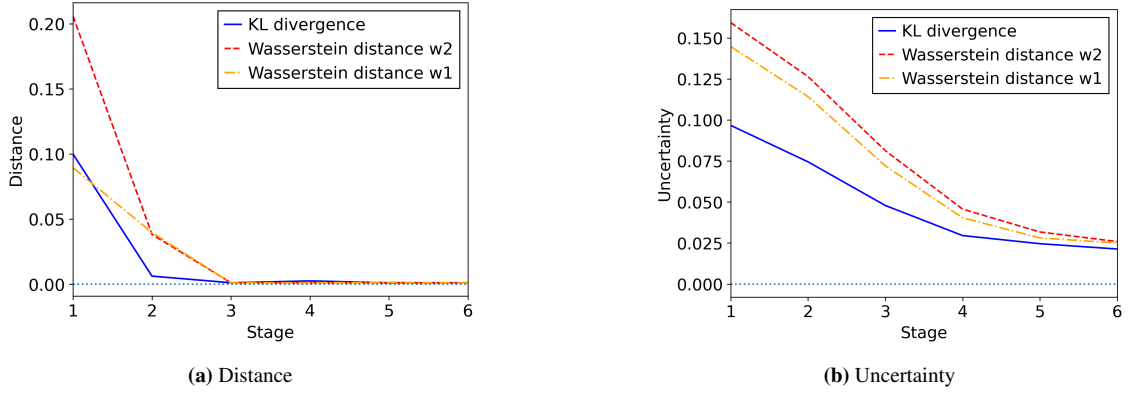


Figure 6: Distance and uncertainty evolution.

It is instructive to discuss the belief updating speed under actual information gain and under expected information gain. Empirically, in stage 1 the posteriors induced by expected-utility designs are less concentrated than those obtained with actual utility (see the first rows of Figs. 5 and 2). And the posterior mass center at the truth by stage 3, which requires one additional measurement relative to the actual-utility setting. The reason is that expected information gain is optimal only in the prior-averaged sense. The design that maximizes the expectation need not be the most informative if evaluating its true information gain, especially when the prior is weak. In other words, the expectation step injects additional uncertainty. This uncertainty propagates across stages because a more diffuse early-stage posterior becomes the prior for later stages, which slows contraction toward the truth.

This additional uncertainty is pivotal when comparing discrepancy measures. Under actual utility, KL divergence typically outperforms the Wasserstein distance: KL favors designs that minimize residual uncertainty and tends to select high-signal, noise-robust measurements, producing

concentrated posteriors. By contrast, Wasserstein distances can be affected by a false-increase effect that shifts designs toward the boundary, leading to more diffuse posteriors. After switching to expected utility, the expectation-induced uncertainty weakens the absoluteness of this ranking. In most cases the expected KL still dominates the expected Wasserstein distance, yet regimes exist in which the Wasserstein-based designs yield lower uncertainty in early stages, owing to the interaction between weak priors and the stage-1 design choice (see Appendix B).

In summary, the false increase effect is still present under expected utilities, predominantly appearing in the early stages and subsequently slowing down the uncertainty reduction in the sequential process due to the residual posterior uncertainty. Because expected utilities introduce additional uncertainty, the design bias of Wasserstein distances does not always translate into a large performance disadvantage. Nevertheless, in most cases, expected KL divergence still achieves better performance than expected Wasserstein distances.

3.3. An inverse problem of convection-diffusion equation with model discrepancy

In this section, we discuss a more challenging case. We assume the model we use is different from the true system, that is, under model discrepancy [50, 45]. In this work, we only consider the parametric error case as our focus is on comparing different metrics. We assume knowing an incorrect source strength parameter $\theta_s = 3$, against the true value 2. Under this setting, it can be expected that normal inference and BED methods can not produce satisfying results. We follow the framework described in Section 2.4 to find designs and iteratively update both the belief of the physical location parameter $\{\theta_x, \theta_y\}$ and the value of the error parameter θ_s .

3.3.1. Case 3: Actual information gain

Figure 7 shows the evolution of the posterior distributions over six stages in the presence of model discrepancy. In stage 1, KL divergence still selects the design at the source location, producing the largest measurement value and the most concentrated posterior. However, because the forward model is incorrect, the posterior does not cover the true parameter but instead forms a ring around it. Despite being misaligned, this posterior is still more compact than those obtained from other measurement locations, which produce larger rings. Designs selected by the Wasserstein metrics are shifted slightly outward relative to KL, resulting in more diffuse posteriors.

Interestingly, in this setting, the Wasserstein-based posterior places more weight on the true source location than the KL-based posterior. As a result, by stage 2, after two experiments, the posteriors of Wasserstein distance center more closely to the true value compared to that of KL divergence. The reason can be traced to the stage 1 posteriors: KL's posterior was overly concentrated in the wrong region due to the model error, leading its stage 2 uncorrected posterior to remain more peaked in areas overlapping its stage 1 prior. As a result, when the model is later corrected, the KL posterior requires more substantial probability mass transport to move toward the truth, while the Wasserstein posterior can be adjusted with less effort. In contrast, the more diffuse Wasserstein posterior spread probability more evenly over a wider area, making it less overconfident in an incorrect location. This behavior is quantitatively visible in Fig. 8, where the distance between the posterior mean and the true source, as well as the updates to the model error parameter, evolve more slowly for KL than for the Wasserstein metrics.

We also note that, because model correction can cause the posterior mass to be displaced relative to the main mass of the prior, evaluating KL divergence and its gradient w.r.t. design in this situation can, in principle, be numerically unstable: if the prior assigns near-zero probability to

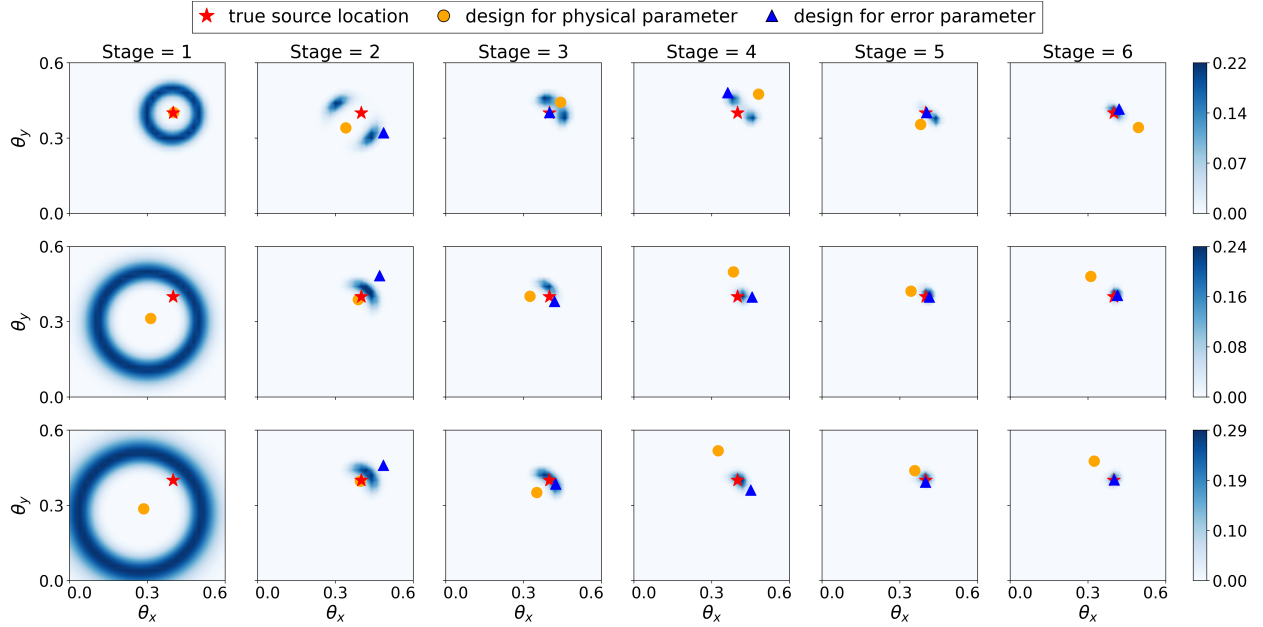


Figure 7: With error (case 3), using actual information gain: posterior. From top to bottom: KL, W_2 , W_1 .

regions where the posterior places mass, $D_{\text{KL}}(p(\theta|y)||p(\theta))$ may diverge. While this instability was not observed in our experiments, it is a theoretical and potential issue.

In summary, under model discrepancy, the false reward effect associated with Wasserstein distances is also observed. However, the presence of model error alters the relative performance: KL’s tendency to concentrate posterior mass in the region favored by the incorrect model makes it overconfident in the wrong location, slowing subsequent corrections. Wasserstein distances, by selecting designs slightly offset from the source location, produce more diffuse and spatially balanced posteriors, which are easier to adjust after the model is corrected. This advantage in correction speed does not imply an inherent superiority of Wasserstein metrics, but within our model correction framework, Wasserstein-based designs could achieve faster and more effective convergence to the truth than those based on KL divergence.

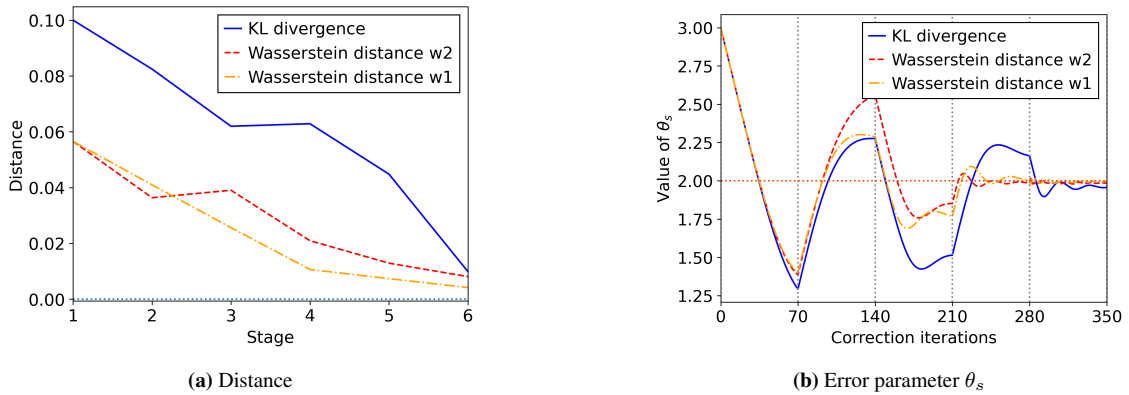


Figure 8: Distance and parametric error evolution.

3.3.2. Case 4: Expected information gain

In this section, we switch to the expected utility functions. Figure 9 shows the reward map at stage 1 under model discrepancy. Again, the design point preferred by the expected Wasserstein distance lies farther toward the boundary than that of the expected KL divergence. Notably, although the result with model discrepancy (Fig. 9) is very similar to that without discrepancy (Fig. 4), they are not the same: with discrepancy, the most favored design is slightly closer to the center. The similarity is because we assume a parametric error, which preserves the model form and thus yields a similar overall pattern.

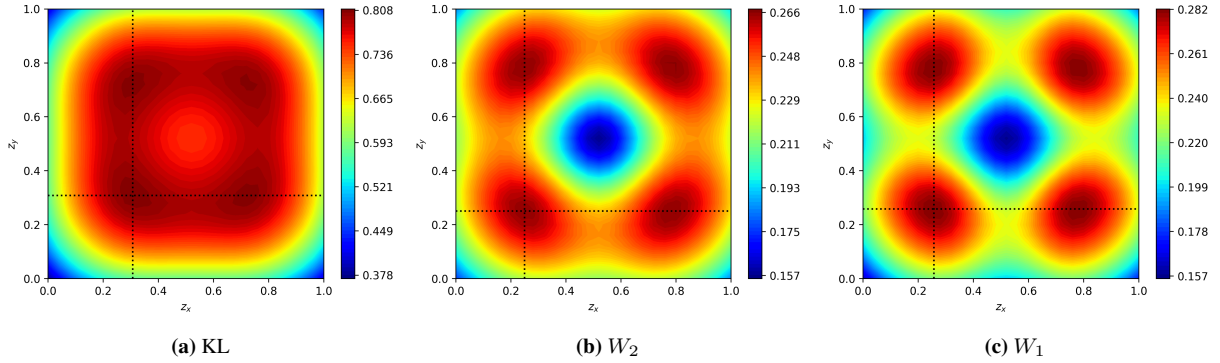


Figure 9: Reward map with model discrepancy.

Figure 10 shows the evolution of the posterior distributions when using expected utility in the presence of model discrepancy (case 4). Both expected utilities exhibit the same vulnerability to model discrepancy as in the actual-utility case: at stage 1, the true parameter lies entirely outside the main posterior mass for both criteria. However, the expected KL divergence produces a sharper posterior, yet model discrepancy drives most probability mass away from the true value. By contrast, the design selected by the expected Wasserstein distance is influenced by the false reward effect and sits farther from the center; its posterior is therefore less concentrated but places higher density on the truth.

In stages 2 and 3, the expected KL divergence continues to prefer over-peaked posteriors located at an incorrect value. Such over-concentration requires more steps to correct through Bayesian updating, so its posterior reaches and covers the truth only by stage 4. The expected Wasserstein distance keeps the main posterior mass closer to the truth throughout the first three stages and already covers the truth by stage 3. A quantitative comparison leads to the same conclusion: the MAP estimate under the expected Wasserstein distance remains consistently closer to the true source than that obtained under the expected KL divergence (see Fig. 11a). These results indicate that, under model discrepancy, the expected Wasserstein distance yields more reliable belief updating than the expected KL divergence.

Figure 11b further reports the evolution of the model-error parameter. When using the expected Wasserstein distance, the discrepancy parameter converges to the true value significantly faster than under the expected KL divergence. The reason is twofold. First, in the early stages, the over-concentrated but mislocated posterior produced by the expected KL divergence yields a poor MAP estimate, which in turn provides a suboptimal input for the discrepancy correction. Second, the slower discrepancy correction feeds back into the inference loop and delays the subsequent posterior refinement. Taken together, the results in this case demonstrate that within our

discrepancy-correction framework, the expected Wasserstein distance yields more effective belief updating and error correction than the expected KL divergence.

In comparison with Section 3.3.1 (actual utility), the underlying mechanism with model discrepancy is similar but not the same. Under the actual-utility setting, Wasserstein distance consistently outperforms KL divergence across our tested configurations. The efficiency of correction hinges on how much uncertainty each utility retains around the truth at early stages: the more uncertainty retained around the truth, the faster the subsequent correction. With expected utilities, however, the outer expectation introduces extra uncertainty. This uncertainty primarily narrows the performance gap between the two criteria, while the expected Wasserstein distance still outperforms the expected KL divergence in most cases.

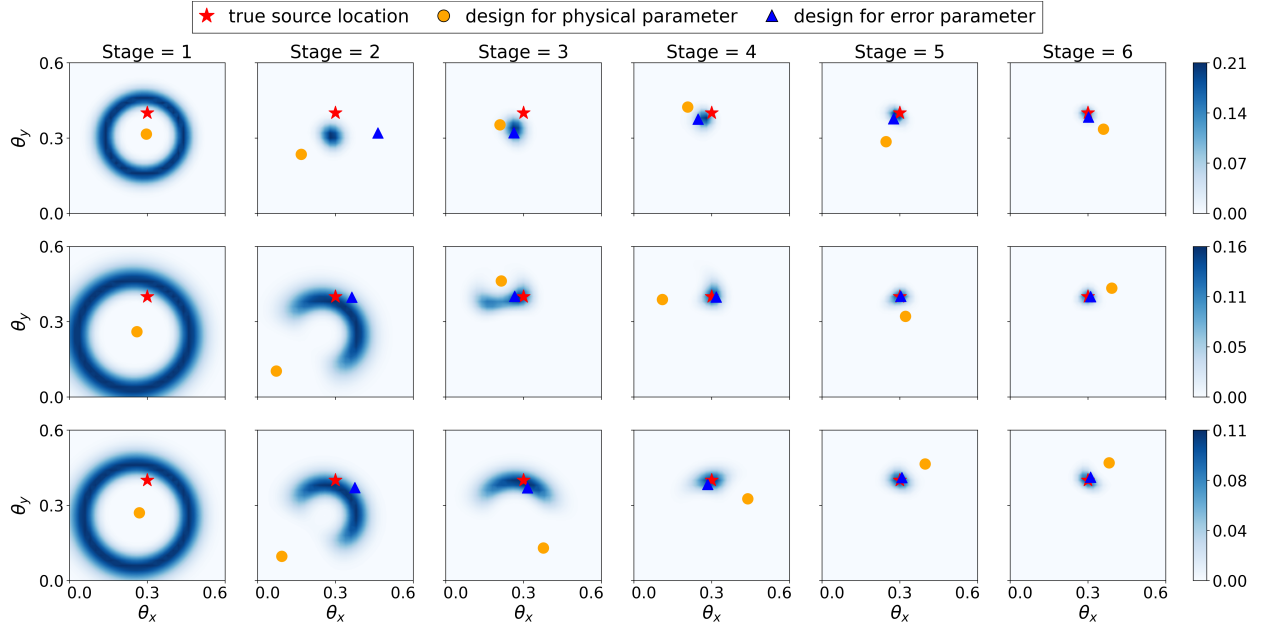


Figure 10: With error (case 4), using expected information gain: posterior. From top to bottom: KL, W_2 , W_1 .

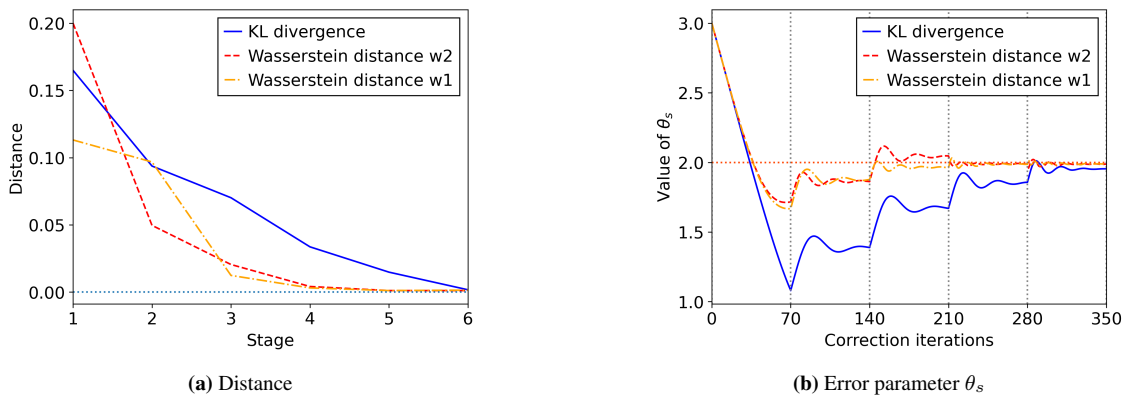


Figure 11: Distance and parametric error evolution.

In summary, when model discrepancy is present, the false increase effect of Wasserstein utilities can still be observed. However, the introduction of expected utilities narrows the relative

performance in probability. In most cases, Wasserstein-based designs leave more balanced uncertainty and thus converge more effectively in both parameter inference and model error updating. Although the expected KL divergence can occasionally outperform the expected Wasserstein distance when the true source happens to appear in certain regions, such cases are relatively rare. Overall, expected Wasserstein utilities provide more reliable performance than the expected KL divergence under model discrepancy.

4. Conclusion

In this work, we first design a toy example to illustrate a potential limitation of Wasserstein distances in BED – the Wasserstein distance is more sensitive to the mean shift of the posterior, especially for a non-informative prior such as uniform distribution. Such a sensitivity can potentially lead to false rewards unrelated to any useful information gain. We then systematically compared Wasserstein distance and KL divergence for utility functions of Bayesian experimental design through a classical source inversion problem. In the absence of model discrepancy, KL divergence provides more effective early-stage designs under actual utilities, producing faster convergence of posteriors toward the truth. On the contrary, Wasserstein distances are affected by location bias and yield more diffuse posteriors. The difference between the two metrics narrows under expected utilities, while the KL divergence still outperforms Wasserstein metrics in most cases. On the other hand, Wasserstein metrics provide a superior performance than the KL divergence if the model discrepancy is non-negligible. More specifically, KL divergence leads to more confident design choices that concentrate posterior mass around incorrect parameter values, while Wasserstein metrics retain more uncertainties in the posterior distribution and thus avoid the convergence to biased results of both physics-based parameters and the model corrections. These results suggest that Wasserstein metrics, though not universally superior, can offer more robust BED results under model discrepancy, while KL divergence tends to be more efficient in BED tasks when the forward model is accurate.

Acknowledgments

H.Y., X.D., and J.W. are supported by the University of Wisconsin-Madison, Office of the Vice Chancellor for Research and Graduate Education with funding from the Wisconsin Alumni Research Foundation.

Data Availability

The data that support the findings of this study are available from the corresponding author upon reasonable request.

References

- [1] Bharath K Sripadur, Kenji Fukumizu, Arthur Gretton, Bernhard Schölkopf, and Gert RG Lanckriet. On the empirical estimation of integral probability metrics. 2012.
- [2] Mark Reid and Robert Williamson. Information, divergence and risk for binary experiments. 2011.
- [3] Leandro Pardo. *Statistical inference based on divergence measures*. Chapman and Hall/CRC, 2018.

- [4] Alison L Gibbs and Francis Edward Su. On choosing and bounding probability metrics. *International statistical review*, 70(3):419–435, 2002.
- [5] Pritam Chanda, Eduardo Costa, Jie Hu, Shravan Sukumar, John Van Hemert, and Rasna Walia. Information theory in computational biology: where we stand today. *Entropy*, 22(6):627, 2020.
- [6] Christoph Adami. Information theory in molecular biology. *Physics of Life Reviews*, 1(1):3–22, 2004.
- [7] Houman Owhadi, Clint Scovel, Timothy John Sullivan, Mike McKerns, and Michael Ortiz. Optimal uncertainty quantification. *Siam Review*, 55(2):271–345, 2013.
- [8] Andrew M Stuart. Inverse problems: a bayesian perspective. *Acta numerica*, 19:451–559, 2010.
- [9] I CSISZAR. Information-type measures of difference of probability distributions and indirect observation. *Studia Scientiarum Mathematicarum Hungarica*, 2:229–318, 1967.
- [10] Friedrich Liese and Igor Vajda. On divergences and informations in statistics and information theory. *IEEE Transactions on Information Theory*, 52(10):4394–4412, 2006.
- [11] Jianhua Lin. Divergence measures based on the shannon entropy. *IEEE Transactions on Information theory*, 37(1):145–151, 2002.
- [12] Bharath K Sriperumbudur, Kenji Fukumizu, Arthur Gretton, Bernhard Schölkopf, and Gert RG Lanckriet. On integral probability metrics, \phi-divergences and binary classification. *arXiv preprint arXiv:0901.2698*, 2009.
- [13] Alfred Müller. Integral probability metrics and their generating classes of functions. *Advances in applied probability*, 29(2):429–443, 1997.
- [14] George Marsaglia, Wai Wan Tsang, and Jingbo Wang. Evaluating kolmogorov’s distribution. *Journal of statistical software*, 8:1–4, 2003.
- [15] Maria L Rizzo and Gábor J Székely. Energy distance. *wiley interdisciplinary reviews: Computational statistics*, 8(1):27–38, 2016.
- [16] M. A. Stephens. *Introduction to Kolmogorov (1933) On the Empirical Determination of a Distribution*, pages 93–105. Springer, New York, NY, 1992.
- [17] Gabriel Peyré, Marco Cuturi, et al. Computational optimal transport: With applications to data science. *Foundations and Trends® in Machine Learning*, 11(5-6):355–607, 2019.
- [18] Cédric Villani et al. *Optimal transport: old and new*, volume 338. Springer, 2008.
- [19] Masahiro Kato, Masaaki Imaizumi, and Kentaro Minami. Unified perspective on probability divergence via the density-ratio likelihood: Bridging kl-divergence and integral probability metrics. In *International Conference on Artificial Intelligence and Statistics*, pages 5271–5298. PMLR, 2023.

- [20] Martin Arjovsky, Soumith Chintala, and Léon Bottou. Wasserstein gan. arxiv e-prints. *arXiv preprint arXiv:1701.07875*, 685, 2017.
- [21] Ilya Tolstikhin, Olivier Bousquet, Sylvain Gelly, and Bernhard Schoelkopf. Wasserstein auto-encoders. *arXiv preprint arXiv:1711.01558*, 2017.
- [22] Luca Ambrogioni, Umut Güçlü, Yağmur Güçlütürk, Max Hinne, Marcel A van Gerven, and Eric Maris. Wasserstein variational inference. *Advances in Neural Information Processing Systems*, 31, 2018.
- [23] Mingxuan Yi and Song Liu. Sliced wasserstein variational inference. In *Asian conference on machine learning*, pages 1213–1228. PMLR, 2023.
- [24] Hongseok Namkoong and John C Duchi. Stochastic gradient methods for distributionally robust optimization with f-divergences. *Advances in neural information processing systems*, 29, 2016.
- [25] Aman Sinha, Hongseok Namkoong, Riccardo Volpi, and John Duchi. Certifying some distributional robustness with principled adversarial training. *arXiv preprint arXiv:1710.10571*, 2017.
- [26] Borja Rodríguez Gálvez, Germán Bassi, Ragnar Thobaben, and Mikael Skoglund. Tighter expected generalization error bounds via wasserstein distance. *Advances in Neural Information Processing Systems*, 34:19109–19121, 2021.
- [27] Jaeho Lee and Maxim Raginsky. Minimax statistical learning with wasserstein distances. *Advances in Neural Information Processing Systems*, 31, 2018.
- [28] Kathryn Chaloner and Isabella Verdinelli. Bayesian experimental design: A review. *Statistical science*, pages 273–304, 1995.
- [29] Dennis V Lindley. On a measure of the information provided by an experiment. *The Annals of Mathematical Statistics*, 27(4):986–1005, 1956.
- [30] Dennis Victor Lindley. *Bayesian statistics: A review*. SIAM, 1972.
- [31] Matthew Jones, Michael Goldstein, Philip Jonathan, and David Randell. Bayes linear analysis for bayesian optimal experimental design. *Journal of Statistical Planning and Inference*, 171:115–129, 2016.
- [32] Tom Rainforth, Adam Foster, Desi R Ivanova, and Freddie Bickford Smith. Modern bayesian experimental design. *Statistical Science*, 39(1):100–114, 2024.
- [33] Xun Huan, Jayanth Jagalur, and Youssef Marzouk. Optimal experimental design: Formulations and computations. *Acta Numerica*, 33:715–840, 2024.
- [34] Elizabeth G Ryan, Christopher C Drovandi, James M McGree, and Anthony N Pettitt. A review of modern computational algorithms for bayesian optimal design. *International Statistical Review*, 84(1):128–154, 2016.

- [35] Howard Raiffa and Robert Schlaifer. *Applied statistical decision theory*. John Wiley & Sons, 2000.
- [36] Morris H DeGroot. *Optimal statistical decisions*. John Wiley & Sons, 2005.
- [37] Paola Sebastiani and Henry P Wynn. Maximum entropy sampling and optimal bayesian experimental design. *Journal of the Royal Statistical Society: Series B (Statistical Methodology)*, 62(1):145–157, 2000.
- [38] Xun Huan and Youssef M Marzouk. Simulation-based optimal bayesian experimental design for nonlinear systems. *Journal of Computational Physics*, 232(1):288–317, 2013.
- [39] Neil Houlsby, Ferenc Huszár, Zoubin Ghahramani, and Máté Lengyel. Bayesian active learning for classification and preference learning. *arXiv preprint arXiv:1112.5745*, 2011.
- [40] Tapani Helin, Youssef Marzouk, and Jose Rodrigo Rojo-Garcia. Bayesian optimal experimental design with wasserstein information criteria. *arXiv preprint arXiv:2504.10092*, 2025.
- [41] Marc C Kennedy and Anthony O’Hagan. Bayesian calibration of computer models. *Journal of the Royal Statistical Society: Series B (Statistical Methodology)*, 63(3):425–464, 2001.
- [42] David J Nott, Christopher Drovandi, and David T Frazier. Bayesian inference for misspecified generative models. *Annual Review of Statistics and Its Application*, 11, 2023.
- [43] Peter Grünwald and Thijs Van Ommen. Inconsistency of Bayesian inference for misspecified linear models, and a proposal for repairing it. *Bayesian Analysis*, pages 1069–1103, 2017.
- [44] Tommie A Catanach and Niladri Das. Metrics for bayesian optimal experiment design under model misspecification. In *2023 62nd IEEE Conference on Decision and Control (CDC)*, pages 7707–7714. IEEE, 2023.
- [45] Huchen Yang, Chuanqi Chen, and Jin-Long Wu. Active learning of model discrepancy with bayesian experimental design. *Computer Methods in Applied Mechanics and Engineering*, 446:118198, 2025.
- [46] Victor M Panaretos and Yoav Zemel. Statistical aspects of wasserstein distances. *Annual review of statistics and its application*, 6(1):405–431, 2019.
- [47] Saurab Chhachhi and Fei Teng. On the 1-wasserstein distance between location-scale distributions and the effect of differential privacy. *arXiv preprint arXiv:2304.14869*, 2023.
- [48] Binshuai Wang, Qiwei Di, Ming Yin, Mengdi Wang, Quanquan Gu, and Peng Wei. Relative-translation invariant wasserstein distance. *arXiv preprint arXiv:2409.02416*, 2024.
- [49] Thibault Séjourné, François-Xavier Vialard, and Gabriel Peyré. Faster unbalanced optimal transport: Translation invariant sinkhorn and 1-d frank-wolfe. In *International Conference on Artificial Intelligence and Statistics*, pages 4995–5021. PMLR, 2022.
- [50] Chi Feng. *Optimal Bayesian experimental design in the presence of model error*. Thesis, Massachusetts Institute of Technology, 2015. Accepted: 2015-07-17T19:46:48Z.

- [51] Jenný Brynjarsdóttir and Anthony O'Hagan. Learning about physical parameters: The importance of model discrepancy. *Inverse problems*, 30(11):114007, 2014.
- [52] Matthew Levine and Andrew Stuart. A framework for machine learning of model error in dynamical systems. *Communications of the American Mathematical Society*, 2(07):283–344, 2022.
- [53] Megan R Ebers, Katherine M Steele, and J Nathan Kutz. Discrepancy modeling framework: Learning missing physics, modeling systematic residuals, and disambiguating between deterministic and random effects. *SIAM Journal on Applied Dynamical Systems*, 23(1):440–469, 2024.
- [54] Xinghao Dong, Chuanqi Chen, and Jin-Long Wu. Data-driven stochastic closure modeling via conditional diffusion model and neural operator. *Journal of Computational Physics*, 534:114005, 2025.
- [55] Jin-Long Wu, Matthew E Levine, Tapio Schneider, and Andrew Stuart. Learning about structural errors in models of complex dynamical systems. *Journal of Computational Physics*, page 113157, 2024.
- [56] Huchen Yang, Xinghao Dong, and Jin-Long Wu. Bayesian experimental design for model discrepancy calibration: An auto-differentiable ensemble kalman inversion approach. *Journal of Computational Physics*, 545:114469, 2026.
- [57] Marco A Iglesias, Kody JH Law, and Andrew M Stuart. Ensemble kalman methods for inverse problems. *Inverse Problems*, 29(4):045001, 2013.
- [58] Yuming Chen, Daniel Sanz-Alonso, and Rebecca Willett. Autodifferentiable ensemble kalman filters. *SIAM Journal on Mathematics of Data Science*, 4(2):801–833, 2022.
- [59] Matthias Gelbrich. On a formula for the l_2 wasserstein metric between measures on euclidean and hilbert spaces. *Mathematische Nachrichten*, 147(1):185–203, 1990.
- [60] Xun Huan and Youssef M Marzouk. Gradient-based stochastic optimization methods in bayesian experimental design. *International Journal for Uncertainty Quantification*, 4(6), 2014.
- [61] Keyi Wu, Thomas O'Leary-Roseberry, Peng Chen, and Omar Ghattas. Large-scale bayesian optimal experimental design with derivative-informed projected neural network. *Journal of Scientific Computing*, 95(1):30, 2023.
- [62] Wanggang Shen and Xun Huan. Bayesian sequential optimal experimental design for non-linear models using policy gradient reinforcement learning. *Computer Methods in Applied Mechanics and Engineering*, 416:116304, 2023.

Appendix A. Derivation of W_2 for Delta Distributions

Before deriving the closed-form expressions for W_2 , we recall why in one dimension the Wasserstein-2 distance can be written in terms of two CDFs (and their inverses), and how those inverses take the explicit piecewise forms below.

1. **CDF and quantile function.** For any probability distribution P on \mathbb{R} :

$$F_P(x) = \Pr_{X \sim P}[X \leq x] \quad \text{is its cumulative distribution function (CDF),}$$

and its *quantile function* (inverse CDF) is defined by

$$F_P^{-1}(u) = \inf\{x : F_P(x) \geq u\}, \quad u \in [0, 1].$$

Intuitively, $F_P^{-1}(u)$ is the location in the real line at which the fraction u of the total probability mass has been accumulated.

2. **One-dimensional optimal transport.** A fundamental theorem in optimal transport on the real line states that the L^2 -Wasserstein distance between two distributions P and Q admits the simple “monotone-rearrangement” formula

$$W_2^2(P, Q) = \int_0^1 (F_P^{-1}(u) - F_Q^{-1}(u))^2 du.$$

Here u plays the role of a “mass coordinate” ranging from 0 to 1.

3. **Why piecewise expressions?**

- For a *delta distribution* $P = \delta_{x_0}$, the CDF jumps from 0 to 1 at x_0 , so

$$F_P^{-1}(u) = x_0, \quad \forall u \in [0, 1].$$

- For the *uniform distribution* $Q = U[-A, A]$,

$$F_Q(x) = \frac{x + A}{2A}, \quad x \in [-A, A],$$

and hence its inverse is the linear map

$$F_Q^{-1}(u) = -A + 2A u, \quad u \in [0, 1].$$

Substituting these explicit quantile functions into the one-dimensional formula yields the piecewise integrals we compute below.

For the three distributions:

- a delta distribution at 0, $\delta(0)$;
- two symmetric delta distributions, $0.5\delta(-\Delta x) + 0.5\delta(\Delta x)$;
- a shifted symmetric delta distribution, $0.5\delta(-\Delta x + \mu) + 0.5\delta(\Delta x + \mu)$, with $\Delta x < A$ and $\Delta x + \mu < A$.

We compute

$$W_2^2(P, Q) = \int_0^1 (F_P^{-1}(u) - F_Q^{-1}(u))^2 du,$$

where $Q = U[-A, A]$ has

$$F_Q^{-1}(u) = -A + 2Au, \quad u \in [0, 1].$$

For a delta distribution $P = \delta(x - x_0)$,

$$F_P^{-1}(u) = x_0 \quad (0 \leq u \leq 1),$$

and one obtains

$$\begin{aligned} W_2^2(\delta_{x_0}, U[-A, A]) &= \int_0^1 (x_0 - (-A + 2Au))^2 du = \int_0^1 (A + x_0 - 2Au)^2 du \\ &= \int_0^1 ((A + x_0)^2 - 4A(A + x_0)u + 4A^2u^2) du \\ &= (A + x_0)^2 - 2A(A + x_0) + \frac{4}{3}A^2 = x_0^2 + \frac{1}{3}A^2. \end{aligned}$$

In particular:

$$W_2^{(1)} = \sqrt{0^2 + \frac{A^2}{3}} = \frac{A}{\sqrt{3}}.$$

For two symmetric deltas $P^{(2)} = \frac{1}{2}\delta_{-\Delta x} + \frac{1}{2}\delta_{+\Delta x}$, the quantile function is

$$F_{P^{(2)}}^{-1}(u) = \begin{cases} -\Delta x, & 0 \leq u < 0.5, \\ +\Delta x, & 0.5 \leq u \leq 1. \end{cases}$$

Hence

$$\begin{aligned} W_2^2(P^{(2)}, Q) &= \int_0^{0.5} (A - \Delta x - 2Au)^2 du + \int_{0.5}^1 (A + \Delta x - 2Au)^2 du \\ &= \Delta x^2 - A \Delta x + \frac{A^2}{3}, \end{aligned}$$

so

$$W_2^{(2)} = \sqrt{\Delta x^2 - A \Delta x + \frac{A^2}{3}}.$$

Finally, for the shifted symmetric deltas $P^{(3)} = \frac{1}{2}\delta_{-(\Delta x - \mu)} + \frac{1}{2}\delta_{+(\Delta x + \mu)}$, one finds

$$W_2^2(P^{(3)}, Q) = \mu^2 + \Delta x^2 - A \Delta x + \frac{A^2}{3},$$

and hence

$$W_2^{(3)} = \sqrt{\mu^2 + \Delta x^2 - A \Delta x + \frac{A^2}{3}}.$$

Appendix B. A reverse case without model discrepancy

Here, we present a representative case in which the source term is located at $\{0.1, 0.1\}$. This location is notably closer to the design generated by the Wasserstein-based criterion (around $\{0.2, 0.2\}$) and farther from that of the KL-based design $\{0.3, 0.3\}$. In this setting, the Wasserstein-based design yields lower uncertainty in the first stage (Fig. B.12), which subsequently leads to consistently smaller uncertainty across all posterior updates (Fig. B.13b).

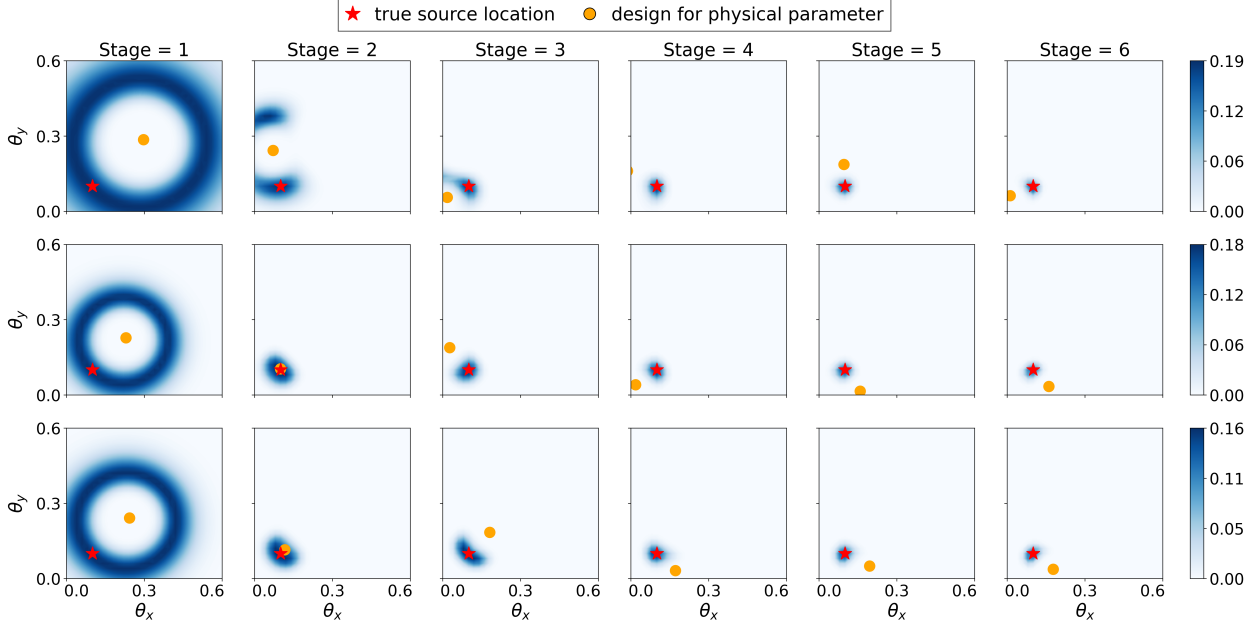


Figure B.12: Without error (case 5), using expected information gain: posterior. From top to bottom: KL, W_2 , W_1 .

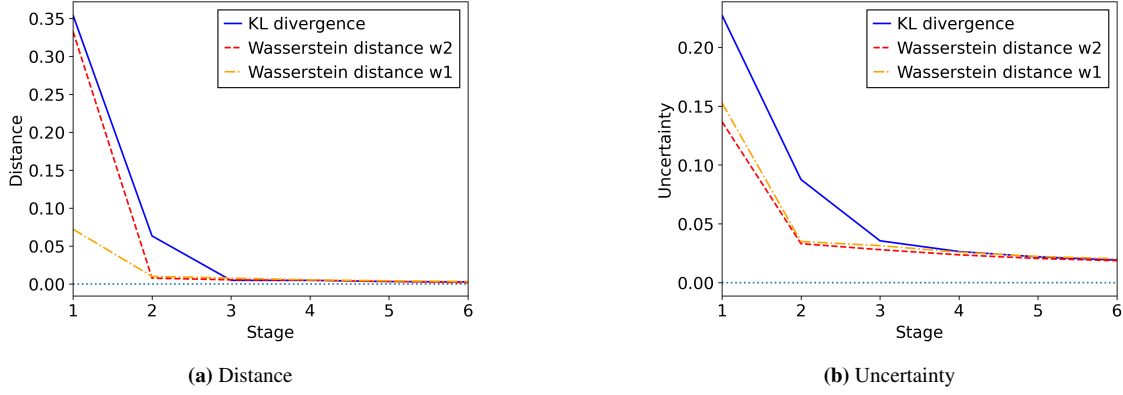


Figure B.13: Distance and uncertainty evolution.

The key factor underlying this behavior is the distance of the source term to the Wasserstein-based design. Geometrically, this implies that the perpendicular bisector of the line segment connecting the KL-based and Wasserstein-based designs partitions the entire square domain into two regions. The lower-left region, where the source term lies in this case, satisfies the condition for which the Wasserstein-based design achieves faster uncertainty reduction during posterior updates. When the source term lies very close to this bisector, the posterior performance of both designs

becomes nearly indistinguishable. This observation further indicates that the region where the Wasserstein-based design outperforms is smaller than that of the KL-based design. Consequently, in the majority of cases without model discrepancy, the KL-based design tends to produce more effective posterior inference.